Interaction of ions and ion clusters with a disordered electron gas: Collective and single-particle excitations

Hrachya B. Nersisyan[1,2,*] Amal K. Das[3,†] and Hrant H. Matevosyan[2]
[1]*Institut für Theoretische Physik II, Universität Erlangen, D-91058 Erlangen, Germany*
[2]*Theoretical Physics Division, Institute of Radiophysics and Electronics, Ashtarak-2, 378410, Armenia*
[3]*Department of Physics, Dalhousie University, Halifax, Nova Scotia B3H 3J5, Canada*
(Received 17 May 2002; published 28 October 2002)

In this paper, we report results on our theoretical studies of stopping power contributions from single-particle and plasmon excitations. We have introduced an equipartition ratio defined as the ratio of stopping contributions from plasmon and single-particle excitations, respectively. Within the linear response theory we have made a comprehensive investigation of this equipartition ratio for fast pointlike and extended projectile ions in a disordered electron gas; the latter is modeled by a degenerate electron gas of metallic densities and with disorder being incorporated within a relaxation-time approximation. As simple but useful examples of pointlike and extended projectiles we have considered proton and He^+ ion, as well as diproton and He^+ ion clusters. We present detailed and comparative results for the equipartition ratio corresponding to several values of the damping parameter which characterizes disorder in our model. The results are also compared, wherever applicable, with those for individual, i.e., uncorrelated projectiles.

DOI: 10.1103/PhysRevE.66.046415 PACS number(s): 52.40.Mj, 34.50.Bw, 61.85.+p, 71.45.Gm

I. INTRODUCTION

One of the important aspects of an interaction of charged particle projectiles in a target medium is the energy loss of the projectiles in the medium. The problem of energy loss of ions and ion clusters in solids is of both theoretical and experimental interests in diverse areas concerning particle-solid interactions [1–11]; more recently energy loss is being studied in connection with energy deposition by ion beams in fusion plasma targets [12–15].

Reliable calculations of energy loss, pioneered by Lindhard [16], have been done (see, Refs. [7,8] for recent reviews) through the linear response theory and by modeling the solid target medium as a dense (degenerate) electron gas. The linear response method is justified for swift charged projectiles [8]. For such high-velocity projectiles or clusters, the energy loss may be mainly due to collective and single-particle excitations in the target medium.

In the linear response approach which assumes a weak coupling between energetic projectiles and the target material, specially a metal, the relevant physical quantities e.g., the stopping power are calculated with the help of the medium dielectric function $\varepsilon(k,\omega)$. The latter contains contribution from both collective and single-particle excitations of the target electrons.

It is of both fundamental and practical interests to study the extent to which the collective and single-particle excitations each contribute to energy loss. For a single *point-ion* projectile, Lindhard and Winther (LW) [17] investigated the respective contributions of these two excitations and found an equipartition sum rule which states that both these excitations contribute equally to energy loss per unit length i.e., stopping power (SP) of the projectile.

In a recent work [18] we have shown that the LW sum rule does not necessarily hold for an extended projectile ion and for ion clusters moving in a degenerate but free (noninteracting) electron gas. We have derived a generalized stopping power sum rule for this type of projectiles. It may be noted that SP has been studied mainly for three types of projectiles: (i) point ion (ii) extended ion and ion clusters, and (iii) structured projectiles having internal structures e.g., atomic shells. In this paper, we shall consider the first two types of projectiles. By an extended ion we refer to the finite size of its charge distribution.

In an earlier work [9], we made a detailed study of various aspects of correlated SP of a diproton cluster by employing different approximations for the linear response function $\varepsilon(k,\omega)$. In both of these studies we considered a degenerate electron gas (DEG) which is free of disorder (e.g., due to impurity etc.). In a real target medium, disorder is expected in various degrees and it affects the decay of the elementary excitations.

To include disorder in a fully interacting electron gas at a microscopic level is rather involved, and no analytical calculations of $\varepsilon(k,\omega)$ without restrictions on k and ω are still available. The effect of disorder has been introduced in $\varepsilon(k,\omega)$ through a phenomenological but number-conserving damping term at the random-phase approximation (RPA) level [19,20]. The resulting $\varepsilon(k,\omega)$ leads to significant changes in the mean free paths and energy losses of low-energy projectiles, as shown by some earlier calculations for electrons and protons interacting with an electron gas [21–24]. The theoretically shown increase in SP (or decrease in mean free path) is due to disorder-induced changes in the plasmon dispersion such that it becomes possible to have plasmon excitation for projectile energies below the threshold predicted in the absence of damping.

The objective of this paper is to report on our studies of

*Electronic address: hrachya@irphe.am
†Electronic address: akdas@dal.ca

the respective contributions of collective (plasmon) and single-particle excitations to individual and correlated SP of point-ion and extended charged projectiles in a disordered DEG, within the linear response approach. The RPA dielectric function which includes damping in a number-conserving relaxation-time approximation (RTA) [19,20] is used for the disordered DEG medium. Within this formalism we briefly present, in Sec. II, the linear response formulation for SP of a dicluster of two identical extended ions and derive analytical expressions for the disorder-inclusive dielectric function. In Sec. III we introduce and formulate two criteria which allow to distinguish between the plasmon and single-particle excitations in the energy-momentum dispersion. These two criteria enable us to reformulate in Secs. III A and III B an equipartition ratio in a disorder-inclusive case. Utilizing these features and with both the criteria we have made detail numerical calculations for the equipartition ratio. The Appendix contains some different and useful results for the plasmon dispersion (within RPA) with and without disorder.

II. LINEAR RESPONSE FUNCTION FORMULATION

In the linear response theory, the SP which is the energy loss per unit length for an external projectile with a spatial charge distribution $\rho_{\rm ext}(\mathbf{r},t)=Q_{\rm ext}(\mathbf{r}-\mathbf{V}t)$ moving with velocity $\mathbf{V}$ in a homogeneous isotropic medium characterized by the dielectric function $\varepsilon(k,\omega)$, is given by [5–11]

$$S=\frac{1}{2\pi^2 V}\int d\mathbf{k}|G(\mathbf{k})|^2\frac{\mathbf{k}\cdot\mathbf{V}}{k^2}\mathrm{Im}\frac{-1}{\varepsilon(k,\mathbf{k}\cdot\mathbf{V})}, \tag{1}$$

where $G(\mathbf{k})$ is the Fourier transform of the stationary charge $Q_{\rm ext}(\mathbf{r})$. We shall consider the range of V for which the linear response theory is adequate [8].

Both the single-particle and collective excitations (i.e., the plasmons) contribute to the SP and these contributions are contained in $\varepsilon(k,\mathbf{k}\cdot\mathbf{V})$ in Eq. (1). In our study the target medium is assumed to be disordered due to impurities etc. As stated in Sec. I, we shall incorporate effects of disorder in $\varepsilon(k,\omega)$ in a somewhat phenomenological manner. This is to include disorder through a relaxation time τ such that the particle number is conserved. This was done first by Mermin [19] and then by Das [20] in the random-phase approximation and in RTA. We refer the reader to Refs. [19,20] for details of this formalism. For $\tau\to\infty$, this linear response function $\varepsilon(k,\omega,1/\tau)$ reduces to the Lindhard dielectric function. In Eq. (1), $\varepsilon(k,\mathbf{k}\cdot\mathbf{V})$ is understood to contain γ $(=1/\tau)$ as a damping parameter due to disorder. The form of $\varepsilon(k,\omega,1/\tau)$ is to be specified shortly.

Equation (1) is applicable to any external charge distribution. For the projectile systems under study we may write $Q_{\rm ext}(\mathbf{r})$ as

$$Q_{\rm ext}(\mathbf{r})=Ze[\,\delta(\mathbf{r})+\delta(\mathbf{r}-\mathbf{R})\,]-e[\,\rho(r)+\rho(|\mathbf{r}-\mathbf{R}|)\,]. \tag{2}$$

For point-ions, only the δ-function terms in Eq. (2) need be considered while for an extended-charge projectile all the terms in Eq. (2) are included. In Sec. III we discuss a dicluster of two identical ions, particularly He^+ ions. $\rho(r)$ is the spatial distribution, assumed to be spherically symmetric, of bound electrons in the ions. Ze is the charge on each of the pointlike ions or nuclei separated by a variable distance $\mathbf{R}$.

We use a $1s$-type wave function of the form

$$\psi_{1s}(\mathbf{r})=\left(\frac{Z^3}{\pi a_0^3}\right)^{1/2}e^{-Zr/a_0} \tag{3}$$

to describe the bound electron on each He^+ ion, with $a_0=0.529$ Å as the Bohr radius. It may be remarked that, unlike in the work of Wang and Nagy [25], we are considering an unscreened $1s$ electron. The Fourier transform of the spatial distribution $\rho(r)=|\psi_{1s}(r)|^2$ is then expressed as

$$\rho(k)=\frac{1}{(1+k^2a_0^2/4Z^2)^2}. \tag{4}$$

For a dicluster of He^+ ions we have

$$|G(\mathbf{k})|^2=2e^2[Z-\rho(k)]^2[1+\cos(\mathbf{k}\cdot\mathbf{R})]. \tag{5}$$

Using Eqs. (1) to (5), the SP of a dicluster can be written as

$$S=2S_{\rm ind}(\lambda)+2S_{\rm corr}(\lambda,R,\vartheta), \tag{6}$$

where $S_{\rm ind}(V)$ and $S_{\rm corr}(\mathbf{R},V)$ stand for individual and correlated SP, respectively. From Eqs. (1) and (5)

$$S_{\rm ind}(\lambda)=\frac{16\Sigma_0}{\pi^3\chi^4\lambda^2}\int_0^\infty\mathcal{Z}^2(\alpha,z)zdz\int_0^\lambda\mathrm{Im}\frac{-1}{\varepsilon(z,u)}udu, \tag{7}$$

$$\begin{aligned}S_{\rm corr}(\lambda,R,\vartheta)=&\frac{16\Sigma_0}{\pi^3\chi^4\lambda^2}\int_0^\infty\mathcal{Z}^2(\alpha,z)zdz\int_0^\lambda\mathrm{Im}\frac{-1}{\varepsilon(z,u)}udu\\&\times\cos\left(\frac{2uz}{\lambda}k_FR\cos\vartheta\right)\\&\times J_0\left(2k_FRz\sin\vartheta\sqrt{1-\frac{u^2}{\lambda^2}}\right).\end{aligned} \tag{8}$$

$J_0(x)$ is the Bessel function of first kind and zero order, and ϑ is the angle between the interionic separation vector $\mathbf{R}$ and the velocity vector $\mathbf{V}$; $\Sigma_0=e^2/2a_0^2\simeq 2.566$ GeV/cm, $\lambda=V/v_F$, $\chi^2=1/\pi k_Fa_0=(4/9\pi^4)^{1/3}r_s$, $r_s=(3/4\pi n_0a_0^3)^{1/3}$, n_0 is the electron gas density, v_F and k_F are the Fermi velocity and wave number of the target electrons, respectively, $\mathcal{Z}(\alpha,z)=Z-\rho(\alpha,z)$. In our calculations χ (or r_s) serves as a measure of electron density. Here, as in Refs. [16,17], we have introduced the following notations $z=k/2k_F$, $u=\omega/kv_F$. In Eq. (6) the term for correlated stopping power $S_{\rm corr}$ vanishes for large $R(R\to\infty)$ and SP is the sum of individual stopping powers for the separate ions. For $R\to 0$ the

two ions coalesce into a single entity. Then $S_{\rm corr}=S_{\rm ind}$, and SP corresponds to that for a projectile of total charge $2e(Z-1)$.

With variables z and u Eq. (4) becomes

$$\rho(\alpha,z)=\frac{\alpha^4}{(\alpha^2+z^2)^2}, \tag{9}$$

where $\alpha=\pi\chi^2 Z$.

Let us now specify the disorder-inclusive dielectric function. With the notations introduced in the preceding paragraph, it reads

$$\varepsilon(z,u)=1+\frac{(zu+i\Gamma)[\varepsilon_{\rm RPA}(z,u,\Gamma)-1]}{zu+i\Gamma[\varepsilon_{\rm RPA}(z,u,\Gamma)-1]/[\varepsilon_{\rm RPA}(z,0)-1]}, \tag{10}$$

where $\Gamma=\hbar\gamma/4E_F$, E_F being the Fermi energy $=\hbar^2k_F^2/2m$ with m as the effective mass. The quantity γ (or Γ) is a measure of damping of excitations in the disordered electron gas. $\varepsilon_{\rm RPA}(z,u,\Gamma)=\varepsilon_{\rm RPA}(k,\omega+i\gamma)$ is the longitudinal dielectric function of zero-temperature (degenerate) electron gas in the RPA. $\varepsilon_{\rm RPA}(z,0)=\varepsilon_{\rm RPA}(k,0)$ is the static dielectric function.

We have analytically evaluated the disorder-inclusive $\varepsilon(z,u)$ for which the results, presented below, appear to be different and we have utilized them in our numerical investigation.

Let us recall the Lindhard (RPA) expression for the longitudinal dielectric function [16]. In variables z and u, it reads as

$$\begin{aligned}\varepsilon_{\rm RPA}(z,u,\Gamma)&=\varepsilon_{\rm RPA}(k,\omega+i\gamma)\\&=1+\frac{\chi^2}{2}\int_0^1 qdq\int_{-q}^{+q}\frac{d\mu}{z^4-(\mu z-zu-i\Gamma)^2}\\&=1+\frac{\chi^2}{z^2}[f_1(z,u)+if_2(z,u)],\end{aligned} \tag{11}$$

where we have introduced the functions $f_1(z,u)$ and $f_2(z,u)$ as in the usual RPA expression of longitudinal dielectric function.

Performing the q and μ integrations in Eq. (11) we obtain, for a nonzero damping,

$$\begin{aligned}f_1(z,u)=\frac{1}{2}+\frac{1}{16z^3}\{&[z^2(U_-^2-1)-\Gamma^2]Y_1(z,U_-)\\&-[z^2(U_+^2-1)-\Gamma^2]Y_1(z,U_+)\\&+4\Gamma z[U_+Y_2(z,U_+)-U_-Y_2(z,U_-)]\},\end{aligned} \tag{12}$$

$$\begin{aligned}f_2(z,u)=\frac{1}{8z^3}\{&\Gamma z[U_-Y_1(z,U_-)-U_+Y_1(z,U_+)]\\&+[z^2(U_-^2-1)-\Gamma^2]Y_2(z,U_-)\\&-[z^2(U_+^2-1)-\Gamma^2]Y_2(z,U_+)\}\end{aligned} \tag{13}$$

with $U_\pm=u\pm z$,

$$Y_1(z,U)=\ln\frac{z^2(U+1)^2+\Gamma^2}{z^2(U-1)^2+\Gamma^2}, \tag{14}$$

$$Y_2(z,U)=\arctan\frac{z(U-1)}{\Gamma}-\arctan\frac{z(U+1)}{\Gamma}. \tag{15}$$

In the case of vanishing damping ($\gamma\to 0$ and $\Gamma\to 0$) the expressions (12)–(15) coincide with the Lindhard result [16].

III. STOPPING POWER AND EXCITATIONS EQUIPARTITION

With the theoretical formalism presented so far, we now take up the main topic of this paper. This is to study how collective and single-particle excitations in the target medium contribute to $S_{\rm ind}$ and $S_{\rm corr}$. This problem was first addressed by Lindhard and Winther [17] for a degenerate electron gas medium without damping ($\gamma=0$). They considered only $S_{\rm ind}$ and only for a point-ion projectile. They formulated an equipartition rule which states that an integral proportional to that in Eq. (7)

$$\mathfrak{I}(u)=\int_0^\infty {\rm Im}\frac{-1}{\varepsilon(z,u)}zdz=\mathfrak{I}_p(u)+\mathfrak{I}_{sp}(u) \tag{16}$$

receives equal contributions from plasmon ($\mathfrak{I}_p$) (with $0<z<u-1$) and from single-particle excitations ($\mathfrak{I}_{sp}$) (with $u-1<z<u+1$), respectively. The functions $\mathfrak{I}_p(u)$ and $\mathfrak{I}_{sp}(u)$ may then be written as

$$\begin{aligned}\mathfrak{I}_p(u)&=\int_0^{u-1}{\rm Im}\frac{-1}{\varepsilon(z,u)}zdz,\\ \mathfrak{I}_{sp}(u)&=\int_{u-1}^{u+1}{\rm Im}\frac{-1}{\varepsilon(z,u)}zdz.\end{aligned} \tag{17}$$

This equipartition rule is valid for sufficiently fast projectile $V>V_t$, where V_t is the threshold ion velocity for plasmon excitation (or $u>V_t/v_F=\lambda_t$). In a recent work [18] we have shown that the LW equipartition rule does not necessarily hold for an extended charged projectile, e.g., a diproton cluster in a degenerate electron gas without disorder ($\gamma=0$). We have established some generalized stopping power sum rules.

We shall now study the equipartition problem for a disordered ($\gamma\neq 0$) electron gas, utilizing, among other things, the results for the linear response function as presented in Eqs. (10)–(15). For our analysis we introduce two criteria which enable us to distinguish, operationally, between contributions

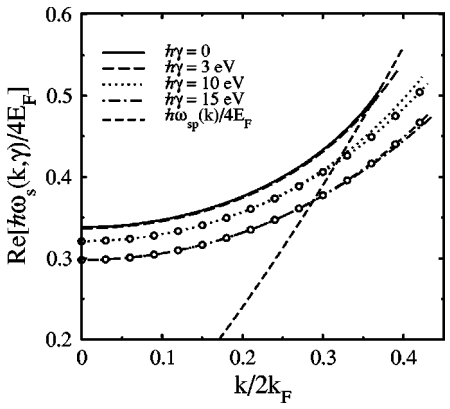

FIG. 1. Real part [$\xi_s = \mathrm{Re}(\hbar\omega_s(k)/4E_F)$] of exact and approximate (the lines with circles) solutions of dispersion equation vs $z = k/2k_F$ for $\hbar\gamma = 0$ (solid line), $\hbar\gamma = 3$ eV (dashed line), $\hbar\gamma = 10$ eV (dotted line), $\hbar\gamma = 15$ eV (dash-dotted line). The short-dashed line corresponds to $\omega = kv_F + \hbar k^2/2m$ (or $\xi_0 = z + z^2$ in units of $\xi = \hbar\omega/4E_F$ and $z = k/2k_F$).

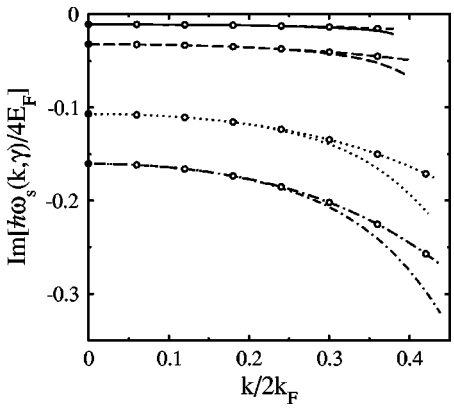

FIG. 2. Imaginary part [$\eta_s = \mathrm{Im}(\hbar\omega_s(k)/4E_F)$] of exact and approximate (the lines with circles) solutions of dispersion equation vs $z = k/2k_F$ for $\hbar\gamma = 1$ eV (solid line), $\hbar\gamma = 3$ eV (dashed line), $\hbar\gamma = 10$ eV (dotted line), $\hbar\gamma = 15$ eV (dash-dotted line).

from plasmon and single-particle excitations. As in the case without damping, we consider the dispersion curve of ω vs k, and look for the intersection at which the plasmon curve first touches the single-particle spectrum; this is criterion 1 ($C1$). The corresponding value of k is denoted by k_c. Figs. 1 and 2 show the solutions $\mathrm{Re}(\omega_s(k,\gamma))$ and $\mathrm{Im}(\omega_s(k,\gamma))$ (in units of $4E_F$) of dispersion equation (DE) $\varepsilon(k,\omega) = 0$ as a function of $z = k/2k_F$, for some values of $\hbar\gamma$. In these figures the lines with circles correspond to approximate solutions of DE [see, the Appendix, Eqs. (A7)–(A10)]. In Fig. 1 the short-dashed line corresponds to single-particle excitation spectrum $\omega_{sp}(k) = kv_F + \hbar k^2/2m$ [or $\hbar\omega_{sp}(k)/4E_F = z + z^2$]. The intersection of single-particle excitation spectrum $\omega_{sp}(k)$ with the real part of plasmon energy $\mathrm{Re}(\omega_s(k,\gamma))$ gives the critical wave number $k_c(\gamma)$.

For $\gamma = 0$ (no disorder), the plasmon will be Landau damped beyond k_c. This means that the plasmon dispersion will have both nonzero real and imaginary parts. But the real part will decay and the imaginary part will increase in strength.

Next we consider the second criterion for characterizing contributions from plasmon and single-particle excitations. We plot the solution for the DE, $\varepsilon(k,\omega) = 0$, for ω with respect to k (see, Figs. 1 and 2). At some value of k, the DE ceases to have either a real or a complex solution. We call this value $k_{\max}(\gamma)$ which provides the second criterion ($C2$)[1]. On physical grounds we expect that $k_{\max}$ is greater than k_c. In the context of stopping, we are assuming that in $C1$, plasmons will not contribute to stopping beyond k_c. This is somewhat restrictive. But let us explore a theoretical model in order to see its consequences. In $C2$, we are assuming that plasmons can still contribute to stopping even when $k > k_c$. Probably this is more realistic. But, again, our idea is to consider two theoretically motivated criteria and compare the physical results which perhaps lie in between the two criteria.

In Fig. 3 we show $z_{\max} = k_{\max}/2k_F$ (solid line) and $z_c = k_c/2k_F$ (dashed line) as a function of $\hbar\gamma$. This figure shows that the critical k_c (in $C1$) decreases monotonically with increasing γ while $k_{\max}$ (in $C2$) increases with γ.

For a further investigation of excitations' equipartition we need to consider an operational definition of the threshold ion velocity for plasmon excitation in a disordered electron gas (in the presence of a nonzero γ). For $\gamma = 0$ (no disorder) we have plasmon excitation within the domain $z < u - 1$. The intersection of the single-particle excitation curve $z = u - 1$ and the plasmon dispersion curve $z_r(u)$ (see the Appendix) gives the threshold value u_t given by $u_t = 1 + z_r(u_t)$; the plasmons are excited only for $u_t \leqslant u \leqslant \lambda$ [Eqs. (7) and (8)]. The threshold ion velocity V_t is related to u_t through $u_t = V_t/v_F$, the latter being denoted by λ_t in subsequent calculations. The value of $z_r(u_t)$ corresponds to the critical wave number $z_c = k_c/2k_F$. In $C1$ we then have the generalization $\lambda_t(\gamma) = V_t(\gamma)/v_F = 1 + k_c(\gamma)/2k_F$ of the threshold ion velocity.

In $C2$ we use the numerical data for plasmon dispersion curves of $\mathrm{Re}(\omega/kv_F)$ and $\mathrm{Im}(\omega/kv_F)$ vs $z = k/2k_F$ for sev-

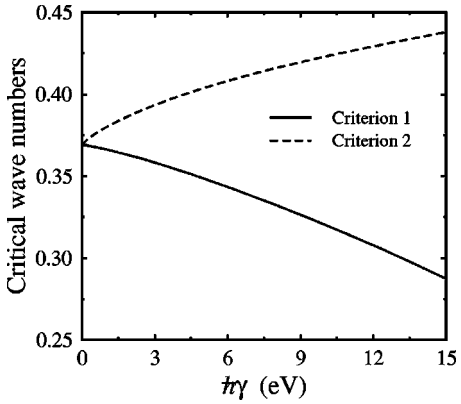

FIG. 3. The critical wave numbers (in units of $2k_F$) vs $\hbar\gamma$ plotted under criterion 1 (solid line) and criterion 2 (dashed line).

[1]After completing this work we became aware that the criterion $C2$ has been applied, in number nonconserving and conserving approximations, to study collective excitations in nuclear matter [26].

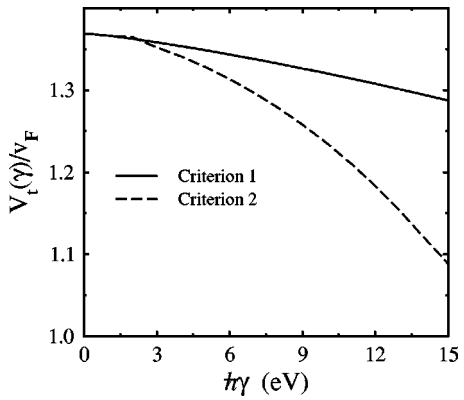

FIG. 4. The threshold ion velocity $V_t(\gamma)$ (in units of v_F) for plasmon excitation vs $\hbar\gamma$ plotted under criterion 1 (solid line) and criterion 2 (dashed line).

eral values of γ, as displayed in Figs. 1 and 2. $C2$ selects the value of $k_{\max}(\gamma)$ at which the dispersion equation has no real or complex solution. In Fig. 4 we have plotted the threshold ion velocities vs $\hbar\gamma$ according to $C1$ (solid line) and $C2$ (dashed line). As expected, both the curves coincide for $\gamma=0$. In this case the threshold ion velocity is found to be

$$V_t \simeq \frac{v_F}{2}+\sqrt{\frac{v_F^2}{4}+\frac{\hbar\omega_p}{2m}}. \tag{18}$$

We now introduce an equipartition ratio (ER) $\Re(\lambda,\Gamma)$ defined as

$$\Re(\lambda,\Gamma)=\frac{S^{(p)}(\lambda,\Gamma)}{S^{(sp)}(\lambda,\Gamma)}, \tag{19}$$

where $S^{(p)}(\lambda,\Gamma)$ and $S^{(sp)}(\lambda,\Gamma)$ are the stopping powers for plasmon and single-particle excitations. $\Re(\lambda,\Gamma)$ describes the strength of plasmon energy loss intensity with respect to a single-particle energy loss intensity. Note that ER $\Re(\lambda,\Gamma)$ vanishes for $V<V_t$ (or $\lambda<\lambda_t$). The ERs corresponding to $C1$ and $C2$ are respectively denoted as $\Re_1(\lambda,\Gamma)$ and $\Re_2(\lambda,\Gamma)$. From Eq. (7) and for an individual ion projectile we find in $C1$

$$S^{(p)}(\lambda,\Gamma)=\int_{\lambda_t(\Gamma)}^{\lambda} u\,du\int_0^{z_c(\Gamma)}\mathcal{Z}^2(\alpha,z)\,\mathrm{Im}\frac{-1}{\varepsilon(z,u)}\,z\,dz, \tag{20}$$

$$S^{(sp)}(\lambda,\Gamma)=\left(\int_0^{\lambda_t(\Gamma)} u\,du\int_0^{\infty} z\,dz+\int_{\lambda_t(\Gamma)}^{\lambda} u\,du\int_{z_c(\Gamma)}^{\infty} z\,dz\right)\times\mathcal{Z}^2(\alpha,z)\,\mathrm{Im}\frac{-1}{\varepsilon(z,u)}. \tag{21}$$

We have omitted the multiplicative factor in Eq. (7) before the integral over z. Similar expressions can be found for the correlated part of ion stopping power. The parameters $z_c(\Gamma)$ and $\lambda_t(\Gamma)$ in Eqs. (20) and (21) are obtained from Figs. 3 and 4, respectively. In a similar manner the ratio $\Re_2(\lambda,\Gamma)$ can be found from Eqs. (19)–(21) by inserting $z_{\max}(\Gamma)$ instead of $z_c(\Gamma)$. The threshold velocity will be defined by numerical data corresponding to the dashed line in Fig. 4.

In the following sections we consider the plasmon and single-particle excitation contributions to SP for pointlike and extended projectiles moving in a disordered electron gas.

A. Equipartition rule for pointlike ions

Using the theoretical and numerical results of Secs. II and III, we have made extensive numerical calculations of ER. Here we consider ER for pointlike ion projectiles. In this case, we need to put $\rho(\alpha,z)=1$ in Eqs. (20) and (21). Consequently, for dimensionless energy losses due to plasmon and single-particle excitations we find the following expressions in $C1$:

$$S^{(p)}(\lambda,\Gamma)=(Z-1)^2\int_{\lambda_t(\Gamma)}^{\lambda} u\,du\int_0^{z_c(\Gamma)}\mathrm{Im}\frac{-1}{\varepsilon(z,u)}\,z\,dz, \tag{22}$$

$$S^{(sp)}(\lambda,\Gamma)=(Z-1)^2\left(\int_0^{\lambda_t(\Gamma)} u\,du\int_0^{\infty} z\,dz+\int_{\lambda_t(\Gamma)}^{\lambda} u\,du\int_{z_c(\Gamma)}^{\infty} z\,dz\right)\mathrm{Im}\frac{-1}{\varepsilon(z,u)}. \tag{23}$$

Let us note that in this case the stopping powers $S^{(p)}(\lambda,\Gamma)$ and $S^{(sp)}(\lambda,\Gamma)$ are proportional to $(Z-1)^2$. Therefore, the ratios $\Re_1(\lambda,\Gamma)$ and $\Re_2(\lambda,\Gamma)$ do not depend on the projectile ion charge Z.

Next we present numerical results for ER. We have used the analytical results presented in the Appendix in order to effect a numerical integration of Eqs. (22) and (23). Figure 5 shows $\Re_1(\lambda,\Gamma)$, i.e., ER, for a single-proton projectile [Fig. 5(a)] and a diproton cluster [Figs. 5(b) and 5(c)] with $R=1$ Å, as a function of V/v_F for six values of the damping parameter γ: $\hbar\gamma=0$ (solid line), $\hbar\gamma=0.1$ eV (dashed line), $\hbar\gamma=1$ eV (dotted line), $\hbar\gamma=3$ eV (dash-dotted line), $\hbar\gamma=10$ eV (dash-dot-dotted line), $\hbar\gamma=15$ eV (short dashed line). The values $\hbar\gamma=0.1$ eV and $\hbar\gamma=1$ eV are comparable with the damping parameter (related to collision time) in Al target. The last value $\hbar\gamma=15$ eV corresponds to the damping parameter in carbon [22–24]. The density parameter is $r_s=2.07$ corresponding to the valence electron density in Al.

We choose two specific values, 0 [Fig. 5(b)] and $\pi/2$ [Fig. 5(c)], for the diproton cluster orientation angle ϑ. Correlations between two protons in the dicluster are maximum and minimum, respectively, for these two values of ϑ. The objective is then to see how, for these maximum and minimum configurations, ER depends on V/v_F and γ. Fig. 5 shows that ER attains noticeably higher values for a diproton cluster. This is due to a correlated motion of the two protons through a resonant interaction with the plasmon excitations in the electron gas. Also the angular dependence of ER is particularly worth noting. It is seen that in the higher velocity range ($V>2v_F$) ER has a remarkably higher value for the larger value of ϑ ($\vartheta=\pi/2$). These features can be explained by noting that the single-particle and collective (plasmon) excitations are effective in different velocity ranges. In a

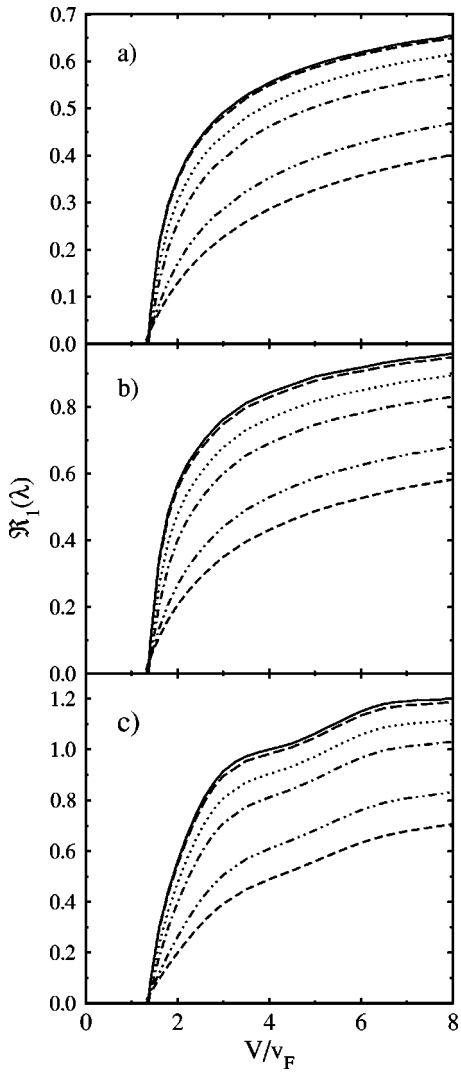

FIG. 5. The ratio $\Re_1(\lambda)$ of a (a) single-proton projectile, (b) diproton cluster with $R=1$ Å, $\vartheta=0$, and (c) $R=1$ Å, $\vartheta=\pi/2$ vs V/v_F for $\hbar\gamma=0$ (solid line), $\hbar\gamma=0.1$ eV (dashed line), $\hbar\gamma=1$ eV (dotted line), $\hbar\gamma=3$ eV (dash-dotted line), $\hbar\gamma=10$ eV (dash-dot-dotted line), $\hbar\gamma=15$ eV (short-dashed line).

small velocity range ($V<2v_F$) the full SP ($S=S^{(p)}+S^{(sp)}$) has a higher value for the larger value of ϑ due to single-particle excitations in this velocity range [10]. In a higher velocity range, the dicluster wake-field excitations become important and we find that the situation is reverse in the higher-velocity range ($V>2v_F$) for which SP for $\vartheta=0$ is larger than for $\vartheta=\pi/2$ [10]. On the other hand, the collective part of SP ($S^{(p)}$) strongly depends on the interparticle distance R. Consequently, a decrease in the full SP at $\vartheta=\pi/2$ may lead to an enhancement of ER at the same value of ϑ.

Another interesting feature is the oscillatory behavior of $\Re_1$ for a diproton cluster with $\vartheta=\pi/2$ and $R=1$ Å in the absence of disorder $\gamma=0$ [see Fig. 5(c), the solid line]. This behavior can be understood as follows: the wavelengths of plasmon excitations along ($\vartheta=0$) and perpendicular ($\vartheta=\pi/2$) to the interproton alignment differ markedly from each other, and these wavelengths also depend on the strength of disorder γ. In order to understand this difference, let us consider a simple plasmon-pole approximation (PPA) [see, e.g., Refs. [3,9,27]] which is a good approximation for the linear response function in a high-projectile-velocity domain, specially when $V>V_p=\sqrt{\hbar\omega_p/2m}\simeq 0.48 r_s^{1/4} v_F$ (where $\hbar\omega_p$ is the plasmon energy). The individual and correlated SP for a diproton cluster within PPA was investigated in Refs. [3,9]. It has been shown that the individual SP, $S_{\rm ind}\sim 2\ln(V/V_p)$, receives equal contributions from plasmon and single-particle excitations. When $\vartheta=0$, for the correlated SP we find [9]

$$S_{\rm corr}\sim\cos\left(\frac{\omega_p}{V}R\right)\ln\left(\frac{V}{V_p}\right)+\frac{1}{2}\left[\mathrm{ci}\left(\frac{V\omega_p}{V_p^2}R\right)-\mathrm{ci}\left(\frac{\omega_p}{V}R\right)\right], \tag{24}$$

where ci(z) is the integral cosin function. The first term in Eq. (24) is the collective part of the SP and the remaining terms correspond to the single-particle excitations. The wavelength of plasmon excitation along the dicluster alignment is $\approx\lambda_1=V/\omega_p$. For single-particle excitations there are two characteristic wavelengths along the dicluster alignment namely λ_1 and also $\lambda_3=V_p^2/V\omega_p$.

When $\vartheta=\pi/2$, the correlated SP from Ref. [9] is proportional to

$$S_{\rm corr}\sim K_0\left(\frac{\omega_p}{V}R\right)-\int_{R/\lambda_2}^{\infty}\frac{dx}{x}J_0(x)+\int_{V_p/V}^{1}\frac{dx}{x}J_0\left(\frac{R}{\lambda_3}x\sqrt{1-x^2}\right), \tag{25}$$

where K_0 is the modified Bessel function, and $\lambda_2=V_p/\omega_p$. When $V>V_p$, the three lengths satisfy the inequality $\lambda_1>\lambda_2>\lambda_3$. The first two terms in Eq. (25) are responsible for plasmon excitations and the third term for single-particle excitations. From Eq. (25) it is seen that the characteristic length scales for plasmons are λ_1 and λ_2, and those for single-particle excitations are λ_2 and λ_3.

From Eqs. (24) and (25) it follows that the dominant wavelength along the dicluster alignment, $\lambda_\parallel$, can be much larger than the corresponding wavelength perpendicular to the alignment, $\lambda_\parallel\gg\lambda_\perp$. As can be seen from Eq. (25), $\lambda_\perp$ also depends on V but it may not be as sensitive to a variation in V (i.e., when $\lambda_\perp\simeq\lambda_2$); it may also decrease with an increasing V (i.e., when $\lambda_\perp\simeq\lambda_3$). For our chosen value of $R=1$ Å and in a high-velocity range, $R\ll\lambda_1$, $R\sim\lambda_2$ ($\lambda_2\sim 0.5$ Å for Al target), and $R\gg\lambda_3$. Therefore, we may expect that $\Re_1$ will not be sensitive to a variation in V for $\vartheta=0$ while for a perpendicular alignment of a dicluster ($\vartheta=\pi/2$) $\Re_1$ exhibits small oscillations with an increasing V.

For further consideration it will be useful to introduce explicit expressions for ER along ($\Re_\parallel^{(\rm PPA)}$) and perpendicular ($\Re_\perp^{(\rm PPA)}$) to the interproton alignment. From Eqs. (24) and (25) we find

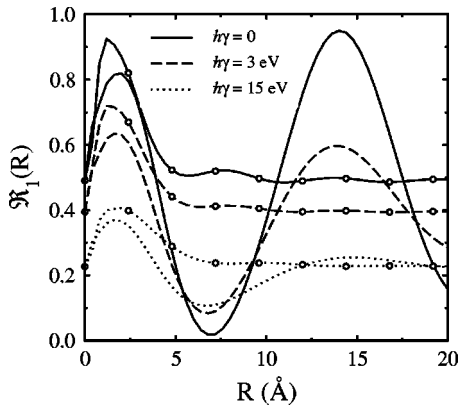

FIG. 6. The ratio $\Re_1$ of a diproton cluster with $V=3v_F$, $\vartheta=0$ (the lines without circles) and $\vartheta=\pi/2$ (the lines with circles), vs R for $\hbar\gamma=0$ (solid line), $\hbar\gamma=3$ eV (dashed line), $\hbar\gamma=15$ eV (dotted line).

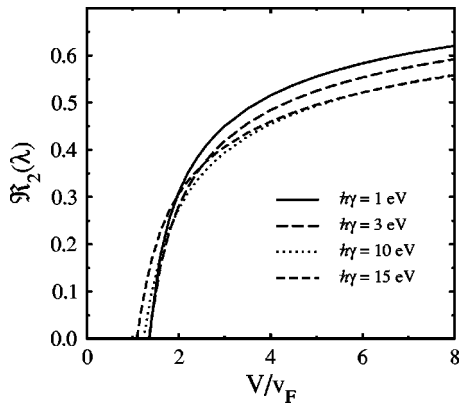

FIG. 7. The ratio $\Re_2(\lambda)$ of a single-proton projectile, vs V/v_F for $\hbar\gamma=1$ eV (solid line), $\hbar\gamma=3$ eV (dashed line), $\hbar\gamma=10$ eV (dotted line), $\hbar\gamma=15$ eV (short-dashed line).

$$\Re_{\parallel}^{(\mathrm{PPA})}(\lambda)=\frac{1+\cos\left(\frac{\omega_p}{V}R\right)}{1+\frac{1}{2\ln(V/V_p)}\left[\mathrm{ci}\left(\frac{V\omega_p}{V_p^2}R\right)-\mathrm{ci}\left(\frac{\omega_p}{V}R\right)\right]}, \tag{26}$$

$$\Re_{\perp}^{(\mathrm{PPA})}(\lambda)=\frac{1+\frac{1}{\ln(V/V_p)}\left[K_0\left(\frac{\omega_p}{V}R\right)-\int_{R/\lambda_2}^{\infty}\frac{dx}{x}J_0(x)\right]}{1+\frac{1}{\ln(V/V_p)}\int_{V_p/V}^{1}\frac{dx}{x}J_0\left(\frac{R}{\lambda_3}x\sqrt{1-x^2}\right)}. \tag{27}$$

For a fixed interproton distance R and in a high-velocity domain ($V\gg\omega_pR$, V_p and V_p^2/ω_pR) we can obtain the following asymptotic values, $\Re_{\parallel}^{(\mathrm{PPA})}(\infty)=1.33$ and $\Re_{\perp}^{(\mathrm{PPA})}(\infty)=1$. Therefore, within PPA and in the high-velocity limit, the ER is larger for a diproton cluster with $\vartheta=\pi/2$. We expect the features, discussed above, to hold generally also beyond PPA.

Next we consider effects of disorder on equipartition. Disorder in the electron gas affects collective excitations in two ways: The plasmon energy $\hbar\omega_p$ decreases (see the Appendix), and the plasmons become damped. These effects are demonstrated in Fig. 5(c) by a monotonic increase in the equipartition ratio $\Re_1$ for nonzero gamma. Besides, in this case it is expected that the wavelength $\lambda_{\parallel}$ will increase with an increasing damping parameter γ.

We have so far presented results for ER vs the projectile velocity V, for a fixed value of the separation distance R. It is of complementary interest to see how the ratio $\Re_1$ behaves as a function of R for a fixed value of V. In Fig. 6 we have plotted $\Re_1$ for a diproton cluster vs R for $V=3v_F$, $\vartheta=0$ (lines without circles) and $\vartheta=\pi/2$ (lines with circles), and for three values of the damping parameter. Figure 6 shows an oscillatory behavior of ER with respect to R. The oscillations are the highest for $\vartheta=0$ and lowest for $\vartheta=\pi/2$. In a more realistic range of R from 1 to 10 Å the plasmon excitation is expected to be more effective at $\vartheta=\pi/2$. This feature has been discussed above. The role of damping is clearly seen in Fig. 6. The wavelengths of oscillations at $\vartheta=0$ increase with γ but the amplitudes are now weaker due to the collisional damping of plasmons.

Having discussed ER for the first criterion ($C1$), we now present results for $\Re_2$, i.e., ER using the second criterion ($C2$). A comparison of SP in $C1$ and $C2$ reveals the following features. In the presence of damping ($\gamma\neq0$), the threshold ion velocity V_t in both $C1$ and $C2$ are noticeably smaller than for $\gamma=0$ (Fig. 4). However V_t in $C2$ is less than V_t in $C1$. Consequently we find that within the framework of $C2$, the plasmon excitation is more effective in some ion velocity range, say $V>V_t$; this is because V_t in $C2$ is smaller than in $C1$. Moreover, the permissible k value ($k_{\max}$) for plasmon excitation is higher in $C2$ than in $C1$ (Fig. 3). The equipartition ratio $\Re_2$ reflects these features. $\Re_2$ is plotted in Fig. 7 for a single-proton projectile. In Fig. 7 the curves are for $\hbar\gamma=1$ eV (solid line), $\hbar\gamma=3$ eV (dashed line), $\hbar\gamma=10$ eV (dotted line), $\hbar\gamma=15$ eV (short-dashed line). The density parameter is the same as for Figs. 5 and 6 ($r_s=2.07$). A comparison of numerical data for both ratios, $\Re_1$ and $\Re_2$, shows that $\Re_1$ is less than $\Re_2$ for any projectile velocity V and damping parameter γ. For $\hbar\gamma$ less than 3 eV the ratio $\Re_1/\Re_2$ differs from unity, although slightly. Specifically, $0.95<\Re_1/\Re_2<1$ for $V>V_t$. There is something interesting about Fig. 7. Like $\Re_1$ [shown in Fig. 5(a)], the ratio $\Re_2$ also decreases with an increasing damping parameter; but in the intermediate velocity range $\Re_2$ may be higher for large damping parameter γ. This is due to the plasmon excitation which is included in that velocity range in $C2$ but not in $C1$ (see, e.g., Fig. 4).

B. Equipartition rule for He^+ ions

We have so far considered ER for pointlike projectiles. Now we will consider ER for extended He^+ ions. The theoretical results for ER have been presented in Sec. III [see Eqs. (20) and (21)] with the function $\rho(\alpha,z)$ given by Eq. (9). It should be noted that for extended projectiles the ratios $\Re_1(\lambda,\Gamma)$ and $\Re_2(\lambda,\Gamma)$ depend on the projectile ion charge Z. For He^+ ion we have $Z=2$.

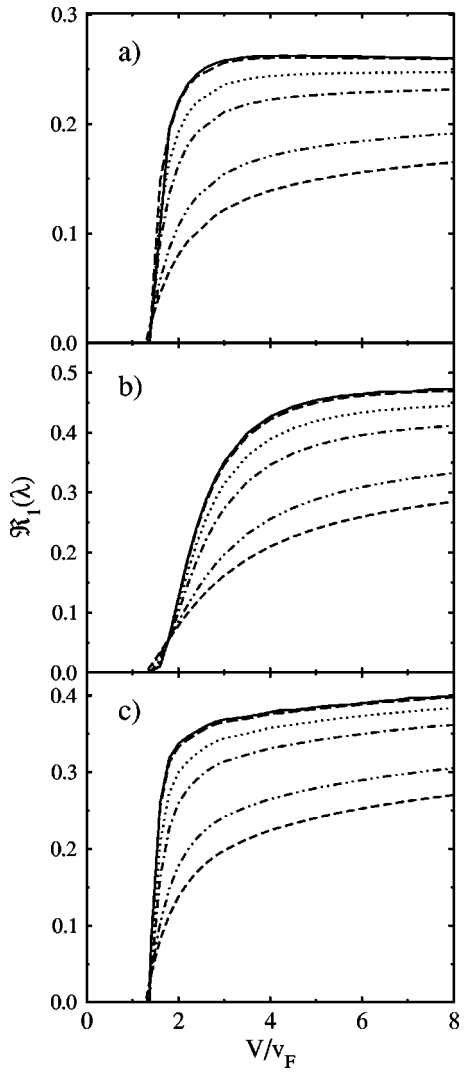

FIG. 8. The ratio $\Re_1(\lambda)$ of a (a) He^+ ion, (b) He^+ ion cluster with $R=3$ Å, $\vartheta=0$, and (c) $R=3$ Å, $\vartheta=\pi/2$ vs V/v_F for $\hbar\gamma=0$ (solid line), $\hbar\gamma=0.1$ eV (dashed line), $\hbar\gamma=1$ eV (dotted line), $\hbar\gamma=3$ eV (dash-dotted line), $\hbar\gamma=10$ eV (dash-dot-dotted line), $\hbar\gamma=15$ eV (short-dashed line).

Next we present the equipartition ratio $\Re_1$ for the electron density parameter $r_s=2.07$. Fig. 8 shows $\Re_1(\lambda,\Gamma)$ for a single He^+ ion projectile [Fig. 8(a)] and for a He^+ ion cluster [Figs. 8(b) and 8(c)] with $R=3$ Å, as a function of V/v_F for six values of damping parameter γ. Here again we choose two values, 0 [Fig. 8(b)] and $\pi/2$ [Fig. 8(c)], of the He^+ ion cluster orientation angle ϑ. Figure 8 may be compared with Fig. 5. It is seen that ER has a remarkably higher value for pointlike projectiles. This is likely due to a correlated motion of the He^+ ion nucleus and the bound electron. Also the difference between velocity dependence of ER for both type of projectiles is particularly worthy noting. For a He^+ ion the curves saturate with increasing V more rapidly than for a proton projectile. In a forthcoming publications [10,11] we shall present asymptotic analytical results for the stopping power of pointlike and extended projectiles in the high-velocity limit. From those results it follows, for instance, that when the damping vanishes the ratio $\Re_1$ for a single-proton tends to unity in the $\lambda\to\infty$ limit, while for a single He^+ ion $\Re_1$ is about $(Z-1)^2/Z^2=0.25$. Note that this result can be retrieved within a binary collision model. It simply states that for close collisions (single-particle excitations), the impact parameter is small. Then the target electrons interact with the unscreened nucleus of He^+ ion with the nuclear charge Z, while for distant collisions (plasmon excitation), the projectile ion can be viewed as a pointlike projectile with total charge $(Z-1)$.

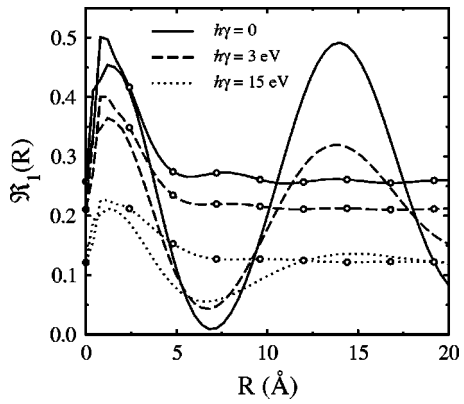

FIG. 9. The ratio $\Re_1$ of a He^+ ion cluster with $V=3v_F$, $\vartheta=0$ (the lines without circles) and $\vartheta=\pi/2$ (the lines with circles), vs R for $\hbar\gamma=0$ (solid line), $\hbar\gamma=3$ eV (dashed line), $\hbar\gamma=15$ eV (dotted line).

There are similarities but also some interesting differences if we compare Figs. 8(b) and 8(c) with Figs. 5(b) and 5(c). For instance, the angular dependence of ER in Figs. 8(b) and 8(c) is reverse to that in Figs. 5(b) and 5(c). In a higher-velocity range ER has a remarkably higher value for an aligned $(\vartheta=0)He^+$ ion cluster. This feature can again be explained by the dominance of single-particle and collective (plasmon) excitations in different velocity ranges.

For a more detailed presentation we show in Fig. 9, $\Re_1$ vs interparticle distance R for a He^+ ion cluster with two values of ϑ: $\vartheta=0$ (lines without circles) and $\vartheta=\pi/2$ (lines with circles). Figure 9 may be compared with Fig. 6, the damping parameters being the same. It is seen that Fig. 9 shows a similar behavior of ER for a He^+ ion cluster although the amplitudes of oscillations are now weaker.

IV. SUMMARY AND CONCLUSION

In this paper, we have presented a detailed theoretical investigation of the contributions of single-particle and collective (plasmon) excitations to the stopping power of point ion, extended ion and ion cluster projectiles in a degenerate electron gas containing disorder. In the course of this study we have also obtained approximate but analytical results for the disorder-inclusive RPA linear response function and for the corresponding plasmon dispersion relations.

We have introduced an equipartition ratio (ER) defined as $\Re=S^{(p)}/S^{(sp)}$ which is the ratio of stopping power contributions from plasmon $(S^{(p)})$ and single-particle excitations $(S^{(sp)})$. These two contributions have been calculated through a generalization of the stopping power integrals given in Eqs. (16) and (17), in order to include disorder in

the linear response function $\varepsilon(z,u)$ and also an extended charged projectile. A further highlight of our work is to introduce two criteria which specify the conditions for plasmon and single-particle excitations as given by the dispersion i.e., the energy-momentum spectrum.

The first criterion $(C1)$ was used earlier [see, e.g., Ref. [17]] for a disorder-free electron gas. We have extended it and applied it in our present investigation. The second criterion $(C2)$ is used in this paper for the first time. Both the criteria are well motivated on physical and theoretical grounds. We have used these two criteria because we do not have a criterion which precisely specifies the conditions for plasmon and single-particle excitations in a disordered DEG. Also a theoretical sum rule (like the Lindhard-Winther equipartition sum rule) is not known for the problem under study. Such a generalized sum rule together with the above-mentioned conditions may be considered as a third criterion $(C3)$ which will be a mathematical formulation for an ''energy-momentum conservation law'' including energy dissipation in the disordered target medium.

By considering an equipartition ratio and some related quantities we have demonstrated that the extent to which single-particle excitations and collective (plasmon) excitations contribute to the stopping power of a fast charged projectile, depends significantly on the charge structure of the projectile and on the disordered or disorder-free nature of the target medium.

Our findings are illustrated by a detailed consideration of pointlike ions in Sec. III A, and of He^+ ions in Sec. III B.

We conclude with these short remarks. In the considerations of the equipartition sum rule we have, as Lindhard and Winther did, modeled a target medium by an electron gas and have ignored possible effects due to energy band structure. A simple and approximate approach to include some energy band effect will be to introduce an experimentally known effective mass. A more immediate aspect is to include some short-range correlation in the linear response function, which we intend to consider in a future work.

ACKNOWLEDGMENTS

It is a pleasure to thank Professor C. Deutsch, Professor P. Sigmund, and Dr. G. Zwicknagel who directed us to some useful references. The authors thank the referee for helpful comments and for bringing Refs. [6,26] to our attention. H.B.N. and H.H.M. would like to thank The Armenian National Science and Education Foundation (ANSEF) for their support and gratefully acknowledge partial financial support by the International Science and Technology Center (Grant No. A-353).

APPENDIX: APPROXIMATE PLASMON DISPERSION WITH AND WITHOUT DAMPING

In order to evaluate the integrals over z in Eqs. (20)–(23) at $\gamma=0$ we shall derive here an approximate solution of the dispersion equation $\varepsilon(z,u)=0$ in the domain $0\leqslant z\leqslant u-1$, $u>1$ where $f_2(z,u)$ vanishes. The integration in this region includes the excitation of collective plasma modes (plasmons) by a fast projectile. Consequently, although $f_2=0$, the integrals in this region are not equal to zero. For a calculation of the collective part of stopping power we use the following known expression [see, e.g., Ref. [28]]:

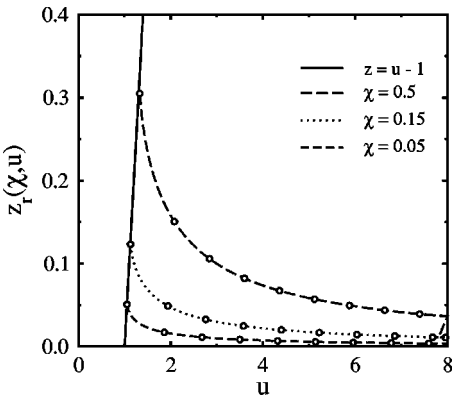

FIG. 10. The exact and approximate (the lines with circles) dispersion curves $z_r(\chi,u)$ without damping ($\gamma=0$) vs u for $\chi=0.5$ (dashed line), $\chi=0.15$ (dotted line), $\chi=0.05$ (short-dashed line). The solid line corresponds to $\omega=kv_F+\hbar k^2/2m$ (or $z=u-1$ in units of $u=\omega/kv_F$ and $z=k/2k_F$).

$$\mathrm{Im}\frac{-1}{\varepsilon(z,u)}\bigg|_{\gamma\to 0}\to \pi z^2\delta(z^2+\chi^2 f_1(z,u)) = \left|\frac{\pi z^2}{2z+\chi^2\partial f_1(z,u)/\partial z}\right|_{z=z_r(\chi,u)} \times\delta(z-z_r(\chi,u)), \tag{A1}$$

where $z_r(\chi,u)$ is the solution of the dispersion equation, which in the case of $\gamma=0$ becomes $z^2+\chi^2 f_1(z,u)=0$. Here the function $f_1(z,u)$ is given by usual RPA expression

$$f_1(z,u)=\frac{1}{2}+\frac{1}{8z}\left[(U_-^2-1)\ln\left|\frac{U_-+1}{U_--1}\right| -(U_+^2-1)\ln\left|\frac{U_++1}{U_+-1}\right|\right]. \tag{A2}$$

We take into account the fact that the function $z_r(\chi,u)$ decreases with an increasing target density (i.e., with a decreasing density parameter χ), and we note that for the metallic target material $(\chi\sim 0.5) z_r\ll u$ [see, e.g., Refs. [9,16] and Fig. 10]. Therefore, the Taylor expansion of the function $f_1(z,u)$ for small z yields the approximate dispersion equation

$$z^2+\chi^2[-f_0(u)-z^2 f_2(u)-z^4 f_4(u)]=0, \tag{A3}$$

where

$$f_0(u)=\frac{u}{2}\ln\left|\frac{u+1}{u-1}\right|-1, \quad f_2(u)=\frac{1}{3(u^2-1)^2},$$

$$f_4(u)=\frac{5u^2+1}{15(u^2-1)^4}. \tag{A4}$$

Equation (A3) has an analytical solution,

$$z_r(\chi,u)=\sqrt{F_1(\chi,u)-\sqrt{F_1^2(\chi,u)-F_2(u)}}, \tag{A5}$$

where

$$F_1(\chi,u)=\frac{1}{2\chi^2 f_4(u)}[1-\chi^2 f_2(u)], \quad F_2(u)=\frac{f_0(u)}{f_4(u)}. \tag{A6}$$

Note that in Eq. (A5) we choose the negative sign in front of the inner square root because only this solution at high $u\gg 1$ leads to the known result $z_r\simeq\chi/u\sqrt{3}$ (see, e.g., Refs. [16,17]). This value of z_r corresponds to the plasmon energy $\hbar\omega_p$ at small k. The another solution of Eq. (A3) is not physical and at large u behaves as $z_r\simeq u^3\sqrt{3}/\chi$.

Figure 10 shows the exact and approximate (the lines with circles) solutions for various values of χ (dashed line, $\chi=0.5$; dotted line, $\chi=0.15$; short-dashed line, $\chi=0.05$). This figure shows that the approximate solution [Eqs. (A5) and (A6)] of dispersion equation is in good agreement with exact numerical results.

Let us now consider the solution of dispersion equation in long-wavelength limit ($z=k/2k_F<1$) for disordered electron gas (with $\gamma\neq 0$). Using the expressions (10)–(15) for the dielectric function in long-wavelength limit we find

$$\zeta(z)=\zeta_0+\zeta_2 z^2+\zeta_4 z^4+\cdots, \tag{A7}$$

where $\zeta=\hbar\omega/4E_F$ [$\xi=\mathrm{Re}(\zeta)$, $\eta=\mathrm{Im}(\zeta)$],

$$\zeta_0=\Omega-\frac{i\Gamma}{2}, \quad \zeta_2=\frac{3\chi^2-2\Gamma^2-4i\Gamma\Omega}{10\chi^2\Omega}, \tag{A8}$$

$$\zeta_4=\frac{(\Omega-i\Gamma/2)^2}{2\Omega^3}\left\{1-\frac{9}{140\chi^2}+\frac{\Gamma^4}{2\chi^4}\left(\frac{1}{4}-\frac{3}{175\chi^2}\right)+\frac{\Gamma^2}{4\chi^2}\left(\frac{87}{350\chi^2}-\frac{11}{3}\right)-\frac{i\Gamma^3\Omega}{2\chi^4}\left(\frac{1}{2}+\frac{6}{175\chi^2}\right)+\frac{i\Gamma\Omega}{\chi^2}\left(\frac{1}{3}+\frac{9}{700\chi^2}\right)\right\}, \tag{A9}$$

$$\Omega=\sqrt{\frac{\chi^2}{3}-\frac{\Gamma^2}{4}}. \tag{A10}$$

It is practically interesting to find the solution of dispersion equation as a function of variable u. Then instead of Eq. (A7) we have

$$\zeta(u)=\zeta_0+\frac{\tilde{\zeta}_2}{u^2}+\frac{\tilde{\zeta}_4}{u^4}+\cdots, \tag{A11}$$

where

$$\tilde{\zeta}_2=\zeta_2\zeta_0^2, \quad \tilde{\zeta}_4=\zeta_0^3(2\zeta_2^2+\zeta_4\zeta_0). \tag{A12}$$

Equation (A11) is applied in our next papers [10,11]. The coefficients ζ_0, ζ_2 and ζ_4 are given by Eqs. (A8)–(A10).

In Figs. 1 and 2 we compare the real and imaginary parts of exact and approximate (the lines with circles) solutions of dispersion equation for $r_s=2.07$ and for some values of γ. These figures also show the good agreement between approximate solution [Eqs. (A7)–(A10)] of dispersion equation and exact numerical results.

When the damping vanishes ($\Gamma=0$, $\eta=0$) the Eqs. (A8)–(A10) become

$$\zeta_0=\frac{\chi}{\sqrt{3}}; \quad \zeta_2=\frac{3\sqrt{3}}{10\chi}; \quad \zeta_4=\frac{\sqrt{3}}{2\chi}\left(1-\frac{9}{140\chi^2}\right). \tag{A13}$$

We can represent the obtained dispersion expression in the usual form

$$\omega^2=\omega_p^2+\frac{3}{5}k^2v_F^2+\left[1+\frac{192}{175}\left(\frac{E_F}{\hbar\omega_p}\right)^2\right]\frac{\hbar^2k^4}{4m^2}, \tag{A14}$$

which differs from the known plasmon-pole expression [see, e.g., Ref. [8]]

$$\omega_{\mathrm{PP}}^2=\omega_p^2+\frac{3}{5}k^2v_F^2+\frac{\hbar^2k^4}{4m^2}. \tag{A15}$$

[1] R.H. Ritchie, C.J. Tung, V.E. Anderson, and J.C. Ashley, Radiat. Res. **64**, 181 (1975); T.L. Ferrel and R.H. Ritchie, Phys. Rev. B **16**, 115 (1977); C.J. Tung and R.H. Ritchie, *ibid.* **16**, 4302 (1977).

[2] N.R. Arista, Phys. Rev. B **18**, 1 (1978).

[3] G. Basbas and R.H. Ritchie, Phys. Rev. A **25**, 1943 (1982).

[4] P.M. Echenique, Nucl. Instrum. Methods Phys. Res. B **27**, 256 (1987).

[5] W. Brandt and M. Kitagawa, Phys. Rev. B **25**, 5631 (1982).

[6] K. Morawetz and G. Röpke, Phys. Rev. E **54**, 4134 (1996).

[7] J.F. Ziegler, J. Appl. Phys. **85**, 1249 (1999).

[8] G. Zwicknagel, C. Toepffer, and P.-G. Reinhard, Phys. Rep. **309**, 117 (1999).

[9] H.B. Nersisyan and A.K. Das, Phys. Rev. E **62**, 5636 (2000).

[10] H.B. Nersisyan and A.K. Das, Phys. Rev. E (to be published).

[11] H.B. Nersisyan and A.K. Das, Nucl. Instrum. Methods B (to be published).

[12] N.R. Arista and W. Brandt, Phys. Rev. A **23**, 1898 (1981); T.A.

Mehlhorn, J. Appl. Phys. **52**, 6522 (1981); N.R. Arista and A.R. Piriz, Phys. Rev. A **35**, 3450 (1987).
[13] C. Deutsch, Ann. Phys. (Paris) **1**, 111 (1986); Laser Part. Beams **2**, 449 (1984); *ibid.* **8**, 541 (1990); Phys. Rev. E **51**, 619 (1995).
[14] J. D' Avanzo, M. Lontano, and P.F. Bortignon, Phys. Rev. E **47**, 3574 (1993).
[15] Proceedings of the 13th International Symposium on Heavy Ion Inertial Fusion, San Diego, CA, 2000, edited by Edward Lee *et al.* [Nucl. Instrum. Methods A **464**, 2001].
[16] J. Lindhard, K. Dan. Vidensk. Selsk. Mat. Fys. Medd. **28**, 1 (1954).
[17] J. Lindhard and A. Winther, K. Dan. Vidensk. Selsk. Mat. Fys. Medd. **34**, 1 (1964).
[18] H.B. Nersisyan and A.K. Das, Phys. Lett. A **296**, 131 (2002).
[19] N.D. Mermin, Phys. Rev. B **1**, 2362 (1970).
[20] A.K. Das, J. Phys. F: Met. Phys. **5**, 2035 (1975).
[21] J.C. Ashley and R.H. Ritchie, Phys. Status Solidi B **83**, K159 (1977).
[22] J.C. Ashley, Nucl. Instrum. Methods **170**, 197 (1980).
[23] J.C. Ashley and P.M. Echenique, Phys. Rev. B **31**, 4655 (1985).
[24] J.C. Ashley and P.M. Echenique, Phys. Rev. B **35**, 8701 (1987).
[25] N.P. Wang and I. Nagy, Phys. Rev. A **55**, 2083 (1997).
[26] U. Fuhrman, K. Morawetz, and R. Walke, Phys. Rev. C **58**, 1473 (1998).
[27] P.M. Echenique, F. Flores, and R.H. Ritchie, Solid State Phys. **43**, 229 (1990).
[28] E.M. Lifshitz and L.P. Pitaevskii, *Physical Kinetics*, 1st ed. (Pergamon Press, Oxford, 1981), Sec. 29, Eq. (29.8).